Disorder and screening in decoupled graphene on a metallic substrate

Sylvain Martin, Sayanti Samaddar, Benjamin Sacépé, Amina Kimouche, Johann Coraux, F. Fuchs, B. Grévin, Hervé Courtois, Clemens Winkelmann

Disorder and Screening in Decoupled Graphene on a Metallic Substrate

S. C. Martin,[1] S. Samaddar,[1] B. Sacépé,[1] A. Kimouche,[1] J. Coraux,[1]
F. Fuchs,[2] B. Grévin,[2] H. Courtois,[1] and C. B. Winkelmann[1]

[1] *Université Grenoble Alpes, Institut NEEL, F-38042 Grenoble, France*
[2] *UMR 5819 (CEA-CNRS-UJF) INAC/SPrAM, CEA-Grenoble, 38054 Grenoble Cedex 9, France*

We report the coexistence of charge puddles and topographic ripples in graphene decoupled from the Ir(111) substrate it was grown on. We show the topographic and the charge disorder to be locally correlated as a result of the intercalation of molecular species. From the analysis of quasi-particle scattering interferences, we find a linear dispersion relation, demonstrating that graphene on a metal can recover its intrinsic electronic properties. The measured Fermi velocity $v_F = 0.9 \pm 0.04 \times 10^6$ m/s is lower than in graphene on dielectric substrates, pointing to a strong screening of electron-electron interactions in graphene by the nearby metallic substrate.

The study of electron-hole puddles in graphene [1, 2] has so far largely focused on graphene sheets isolated by mechanical exfoliation of graphite on dielectric substrates such as SiO_2. The origin of these has been subject to debate, as different studies have pointed to either charged impurities between graphene and SiO_2 [2, 3], others invoking in addition the mixing of the π and σ orbitals due to local curvature [4–9]. In this context, the limited knowledge about the graphene/SiO_2 interface and the ensuing low graphene mobility calls for the use of other substrates. Experiments based on different dielectric environments, that is, different strengths of charged impurities' screening, have been performed. They however showed no significant influence of the substrate dielectric constant on the graphene electronic properties, thereby questioning the role of charged impurities for the puddle formation [10, 11].

On metallic supports, the origin of charge disorder might be very different. Periodic ripples, arising from the lattice parameter mismatch between graphene and most transition metal surfaces, were for instance correlated to Local Density of States (LDOS) variations [12] in graphene on Ru(0001). It however turned out that charge carriers in this system do not exhibit Dirac fermion-like properties, due to a strong hybridization between the $4d$ Ru and p_z C orbitals [13, 14]. Even in less strongly coupled systems, interaction between graphene's conduction/valence bands with surface states of the metal [15, 16] cannot be excluded. A linear dispersion relation in the electronic band structure at the Brillouin zone corners was recovered in graphene on Ru(0001) intercalated with an atomic layer of oxygen below the graphene [17]. This layer unfortunately suppresses the graphene ripples, which prevents from addressing the possible relationship between puddles and topography.

In this work, we report on a STM/STS study of corrugated graphene lying on an Ir metallic substrate, after exposure to ambient air conditions. The analysis of the quasi-particle interference pattern reveals the linear dispersion relation of the graphene band structure, and demonstrates the absence of hybridization with the Ir substrate. Despite the immediate proximity of the metal that acts as an electrostatic screening plate, we observe electron-hole puddles close to the charge neutrality point, akin to those observed on graphene on dielectric substrates. Furthermore, the topographic images of the ripples exhibit strong spatial correlations with charge density inhomogeneities.

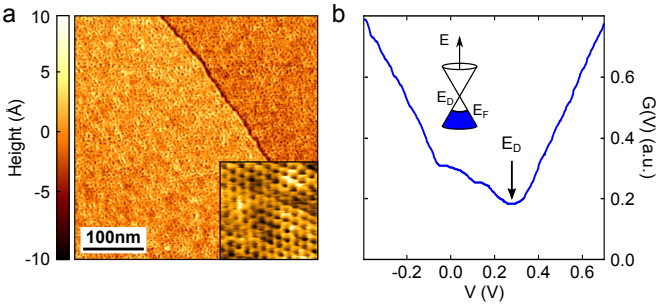

FIG. 1. (a) Scanning tunneling micrograph on graphene on Ir(111). The image size is 400×400 nm^2, tunnel current $I = 1$ nA, bias voltage $V = 0.57$ V). The atomic step in epitaxial Ir(111) covered by graphene is 2.5 Å high. Inset: zoom-in (2.3×2.3 nm^2) atomic resolution image, $I = 1$ nA, V=0.01V. (b) Local tunneling spectroscopy $G(V) = dI/dV$. The Dirac point ($eV = E_D$, arrow) is defined by the minimum of G.

Our experimental set-up is a home-made scanning probe microscope operating at very low temperatures (130 mK). Local tunnel conductance data were obtained using the lock-in technique ($V_{AC} = 6$ mV, $f = 407$ Hz). Samples are heated to 70°C while pumping the chamber and during cryostat cool-down, in order to avoid cryosorption of residual gases. The studied sample is graphene prepared by chemical vapor deposition (CVD) on epitaxial Ir(111) under ultra-high vacuum (UHV), as described in [18]. The samples are exposed to air between the growth and STM inspection. This produces a decoupling of the graphene from its metallic support by oxygen intercalation, transforming the moiré pattern into a disordered topographic landscape [19] (see also Supp. Info.). Figure 1a shows the topography of graphene on a plain Ir atomic terrace. A disordered topographic land-

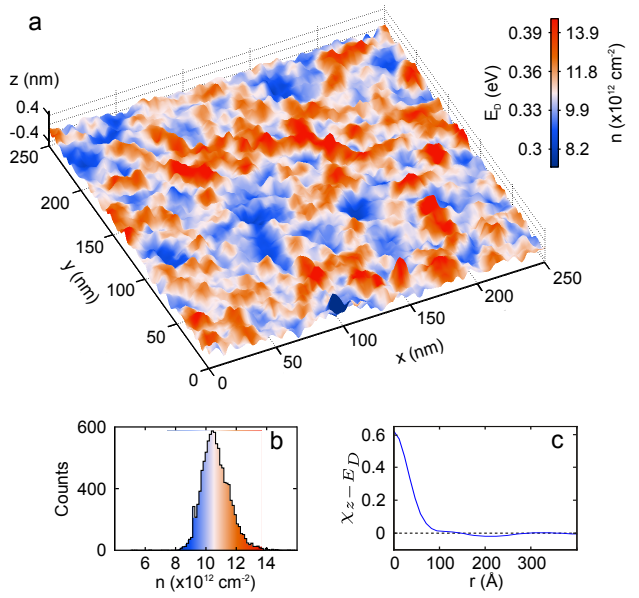

FIG. 2. (a) Dirac point map (color code) superimposed with a 3D plot of the long-wavelength topography. Image of 250×250 nm^2. (b) Carrier density distribution extracted from (a) (see text). (c) Angular average $\chi_{z-E_D}(|\mathbf{r}|)$ of the cross-correlation function (see text) between the above E_D and topography maps.

scape with a typical rms roughness $\sigma_z \approx 50-100$ pm is observed, comparable to the corrugation of graphene on SiO_2 [2]. While the usual moiré pattern is absent, atomic resolution is routinely achieved, demonstrating the cleanliness of the surface.

The electronic LDOS can then be accessed in STM by the measurement of the local tunneling conductance $G(V) = dI/dV$. The tunnel spectra display a V-shape (Fig. 1b), characteristic of the density of states of graphene and similar to data observed by STS on exfoliated graphene on SiO_2 [20, 21]. The voltage V_{min} at the conductance minimum has been identified in previous works [2] as the charge neutrality point, that is, the Dirac point in graphene at energy $E_D = eV_{min}$. The value of E_D reflects the strength of the local graphene doping [2, 4, 20], which is p-type here. A dip of width of about 20 meV is also present around zero bias, which is frequently reported in STS studies on graphene [20–22] and will not be discussed in this work. We have measured a series of high-resolution conductance maps at low temperature. At each position $\mathbf{r}$ of a tunnel conductance map, the Dirac point energy E_D is extracted using a parabolic fit around the minimum of G. The average doping (sample dependent by ±10%) is found to be $E_D^0 = 340$ meV in Fig. 2a. This is somewhat larger than that of the same system in undisrupted UHV conditions (≈ 100 meV) [15], and lesser than that achieved therein by controlled and exclusive intercalation of oxygen (≈ 500 meV) [23].

The map shown in Fig. 2a pictures the spatial inhomogeneities of E_D around its mean value, forming a smooth landscape of charge puddles, of about 8-9 nm in diameter. From the relation $E_D^2 = (\hbar v_F)^2 \pi n$ [3], where $\hbar$ and v_F are the reduced Planck constant and the Fermi velocity respectively, we deduce the distribution of the charge carrier density n (Fig. 2b), where we take $v_F = 0.9 \times 10^6$ m/s as will be discussed later. Notably, the standard deviation $\sigma_n \approx 1.2 \times 10^{12}$ cm^{-2} is slightly higher than in graphene exfoliated on SiO_2 ($\approx 4 \times 10^{11}$ cm^{-2}) [2, 24]. We further note that the puddle radius is very close to the Thomas-Fermi screening length which can be evaluated [3] as $\lambda_{TF} \approx 1.1 \times n^{-1/2} \approx 3.4$ nm.

We now focus on the comparison between the Dirac point distribution and the topography. Since only topographic variations at length scales similar or larger than the typical puddle size can correlate with the charge inhomogeneities, we filter out the topographic maps from structures of dimensions below half the mean puddle size. Figure 2a shows the superposition of an $E_D(\mathbf{r})$ map (color scale) along with the long wavelength-pass filtered topography $z(\mathbf{r})$ recorded at the same position (3D profile). A very high degree of correlation between doping and topography is readily seen. We have quantified this by calculating the normalized cross-correlation function $\chi_{z-E_D}(\mathbf{r}) = \sum_i E_D(\mathbf{r_i} - \mathbf{r}) \times z(\mathbf{r})/(\sigma_{E_D} \times \sigma_z)$ of the two data sets. The local cross-correlations $\chi^0_{z-E_D}$ between $z(\mathbf{r})$ and $E_D(\mathbf{r})$ are in excess of 60 % in large area maps (Fig. 2c). These correlations are independent on the region chosen, but are enhanced in maps with dimensions much larger than the typical puddle size. When correlating spectroscopic maps with topography, one also has to recall that in constant-current STM mode a LDOS variation will lead to a change in the tip-sample distance z. This can misleadingly induce phantom topographic features. We have carefully analyzed such possible LDOS contribution to the topography and shown them to be much smaller than the observed corrugation (see Supp. Info. for details).

The above analysis therefore leads to the conclusion that disordered graphene on a metallic substrate displays a strong local correlation between doping and topography. Several scenarios can be considered for this observation. A contribution of curvature effects [5–8] could for example be anticipated. In the present system, the theoretically expected contribution of this effect is however nearly two orders of magnitude below the observed amplitude of the doping disorder [25]. The graphene doping could further be due to graphene-metal distance dependent charge transfer from the metallic substrate due to finite electronic wave function overlap. Calculations of this effect [26] yield a qualitatively correct description, including the correct sign of $\chi^0_{z-E_D}$ for graphene on iridium. Scanning probe measurements at the boundary between coupled and uncoupled graphene on iridium have however shown the graphene to iridium distance to in-

crease by about 1 nm upon decoupling [19], a distance at which the above scenario would have negligible contributions. The most likely explanation of the doping bases on the presence of molecular species intercalated between the graphene and its substrate [19, 23]. Locally enhanced accumulation of negatively charged intercalates induce a reduction of the Fermi level, that is, enhanced p-doping in the graphene. It has indeed been shown that oxygen intercalation at high temperatures could reversibly modify both the graphene doping and its hybridization to the substrate [23].

In order to obtain a more microscopic understanding of the role of the local electrostatic environment as electron scattering centers, we have tracked the wave vector $\mathbf{k}$ distribution of interference patterns in the Fourier transforms of LDOS maps. The evolution of the dominant $\mathbf{k}$, relative to the Brillouin zone corner, as a function of the energy level of each map then reflects the dispersion relation of the scattered electrons. In graphene, both the large k intervalley and the small k intravalley scatterings have been observed by this technique [27]. For intravalley scattering, the wave vector transfer $\mathbf{q}$ links two points of the circle resulting from the intersection of a given Dirac cone and a constant energy plane. A particular characteristic of graphene is the suppression of low-energy backscattering [28]. One therefore expects a smooth distribution of q between 0 and $2k_F$ for intravalley scattering, seen as a disk in reciprocal space.

In our data, the LDOS maps at energies far from E_D^0 display clearly resolved structures at length scales smaller than the typical puddle size (Figs. 3a–f). Further, the size of the observed features decreases with increasing $|E-E_D^0|$. The Fourier transform maps display a disk-like structure (Fig. 3g) from which we extract $k = q_{max}/2$ at each energy (Fig. 3h). The radius $q_{max}/2$ of the interference patterns is defined as the inflection point of the angular averaged Fourier intensity, that is, the minimum of its smoothed derivative. This criterion produces the $k(E)$ dispersion with least noise but also slightly overestimates the wave vectors involved by adding a constant shift [2] to the detected values of q, which results in the linear dispersion bands crossing at $k > 0$ in Fig. 3h.

The experimental dispersion relation at small k has the features of graphene close to the Dirac point, evidencing thus the scattering mechanism at work as intravalley. A fit by the linear dispersion relation of graphene $E = E_D^0 \pm \hbar v_F k$ (Fig. 3h) yields $v_F = 0.90 \pm 0.04 \times 10^6$ m/s. In unhybridized graphene, v_F is a sensitive probe of the strength of electron-electron interactions [3, 29], which can be screened by a large dielectric constant ϵ environment. While a Fermi velocity$v_F = 2.5 \times 10^6$ m/s has been reported on a low-ϵ quartz substrate [30], it decreases to about $1.1 - 1.4 \times 10^6$ m/s on SiO_2 [2, 21], with a limiting value of about 0.85×10^6 m/s expected for infinite screening [30, 31]. The present system can actually be envisaged as graphene on a dielectric substrate

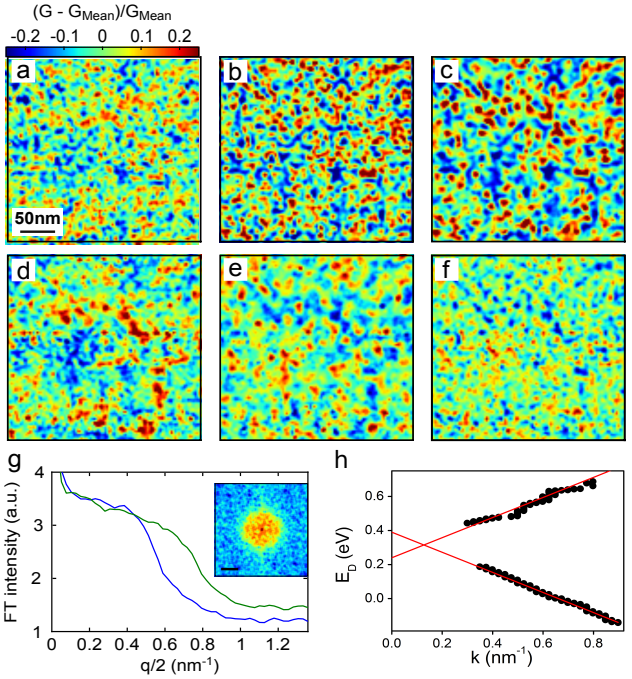

FIG. 3. (a) - (f) $G(\mathbf{r}, E)$ maps for $E = -185; 15; 125; 345; 555$ and 700 meV respectively. The color scale is set to cover fluctuations of ± 25 % with respect to the average G at a given E. As the Dirac point is approached, the islands size can no longer be resolved. (g) Power spectral density from angular averaging of Fourier transform of (b) (blue) and (c) (green). The inset shows the Fourier transform of (b). The scale bar is 0.5 nm^{-1}. (h) Energy - wave vector relation extracted from Fourier analysis of the density of states maps at energy E. The dashed lines are fits to the linear dispersion relation of graphene, yielding $v_F = 0.90 \pm 0.04 \times 10^6$ m/s and $E_D^0 = 0.32$ eV.

with divergent ϵ. In spite of the rather high doping level, the Thomas-Fermi screening length λ_{TF} remains larger than the graphene-iridium distance. One can thus reasonably assume the substrate screening to dominate over the intrinsic screening of the graphene, although highly doped. With the above analysis it is thus seen that (i) the linear dispersion relation of graphene decoupled from a metallic substrate survives at both positive and negative energies and (ii) electron-electron interactions in the graphene sheet are strongly screened.

One remaining open question concerns the physical origin of the observed quasi-particle scattering. It is tempting to question localization-type interpretations to explain the LDOS features in real space in Fig. 3. We have studied the variations of the features studied above (puddles and interference patterns) as a function of magnetic field and found no significant change of neither the E_D nor the G maps up to the maximum experimental magnetic field of 2 T (Fig. 4). For symmetry reasons, Anderson localization is indeed not expected in graphene in the absence of atomically sharp defects providing intervalley

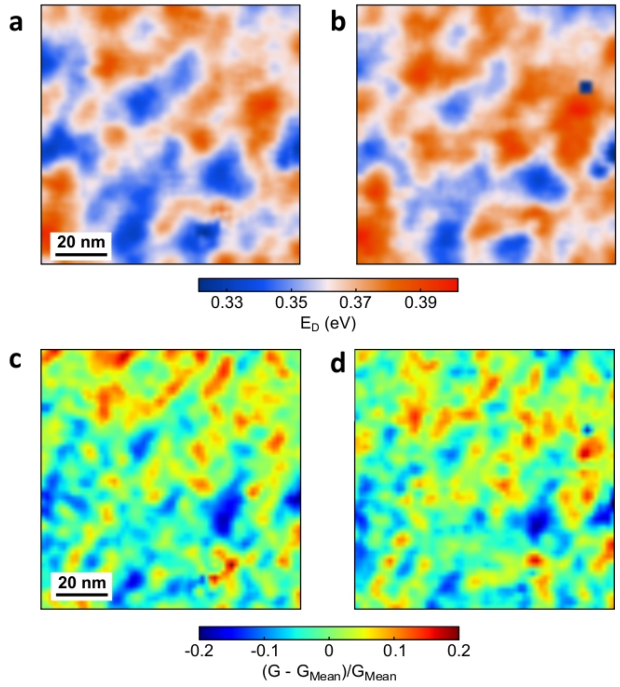

FIG. 4. Dirac point map at zero magnetic field (a) and at $B = 2$ T (b). Density of states map at $E - E_D = -330$ meV at zero magnetic field (c) and $B = 2$ T (d). All four maps are taken over the same region at $T = 130$ mK.

coupling [3]. The magnetic field-independence of the observed patterns therefore completes the picture of long-range Coulomb interactions generating quasi-particle interferences through intravalley scattering.

In conclusion, the present work demonstrates that CVD grown graphene can be completely decoupled from its metallic substrate, displaying local properties that are very similar graphene on a dielectric substrate like SiO_2. The main contrasting feature with respect to the latter system is that the dopants here indeed have a topographic signature. We observe a linear electronic dispersion relation, demonstrating unhybridized graphene with highly screened electron-electron interactions. While the coupling constant of graphene, that is, the ratio of interaction to kinetic energy $\alpha \propto (\epsilon v_F)^{-1}$, is of order unity in unscreened graphene [29], studying graphene in a large and adjustable dielectric constant environment could allow for tuning α.

This work was supported by the ANR-2010-BLAN-1019-NMGEM and EU-NMP3-SL-2010-246073 GRENADA contracts. The authors are indebted to A. Tomadin, M. Gibertini, F. Guinea and M. Polini for their estimation of the influence of curvature effects. We further thank L. Magaud, P. Mallet, J.-Y. Veuillen, V. Guisset, V. Bouchiat and P. David for help and stimulating discussions.

[1] J. Martin, N. Akerman, G. Ulbricht, T. Lohmann, J. H. Smet, K. von Klitzing, and A. Yacoby, Observation of electron-hole puddles in graphene using a scannin single-electron transistor, Nature Phys. **4**, 144 (2007).
[2] Y. Zhang, V. W. Brar, C. Girit, A. Zettl, and M. F. Crommie, Origin of spatial charge inhomogeneity in graphene, Nature Phys. **5**, 722 (2009).
[3] S. Das Sarma, S. Adam, E. H. Hwang, and E. Rossi, Electronic transport in two-dimensional graphene, Rev. Mod. Phys. **83**, 407 (2011).
[4] A. Deshpande, W. Bao, F. Miao, C. Lau, and B. LeRoy, Spatially resolved spectroscopy of monolayer graphene on SiO_2, Phys. Rev. B **79**, 205411 (2009).
[5] D. Gazit, Correlation between charge inhomogeneities and structure in graphene and other electronic crystalline membranes, Phys. Rev. B **80**, 161406(R) (2009).
[6] M. Gibertini, A. Tomadin, M. Polini, A. Fasolino, and M. I. Katsnelson, Electron density distribution and screening in rippled graphene sheets, Phys. Rev. B **81**, 125437 (2010).
[7] M. Gibertini, A. Tomadin, F. Guinea, M. I. Katsnelson, and M. Polini, Electron-hole puddles in the absence of charged impurities, Phys. Rev. B **85**, 201405 (2012).
[8] E.-A. Kim and A. H. Castro Neto, Graphene as an electronic membrane, Europhys. Lett. **84**, 57007 (2008).
[9] P. Partovi-Azar, N. Nafari, and M. R. Tabar, Interplay between geometrical structure and electronic properties in rippled free-standing graphene, Phys. Rev. B **83**, 165434 (2011).
[10] L. A. Ponomarenko, R. Yang, T. M. Mohiuddin, M. I. Katsnelson, K. S. Novoselov, S. V. Morozov, A. A. Zhukov, F. Schedin, E. W. Hill, and A. K. Geim, Effect of a High-κ Environment on Charge Carrier Mobility in Graphene, Phys. Rev. Lett. **102**, 206603 (2009).
[11] N. J. G. Couto, B. Sacépé, and A. F. Morpurgo, Transport through Graphene on $SrTiO_3$, Phys. Rev. Lett. **107**, 225501 (2011).
[12] A. L. Vázquez de Parga , F. Calleja, B. Borca, M. C. G. Passeggi, Jr., J. J. Hinarejos, F. Guinea, and R. Miranda, Periodically Rippled Graphene: Growth and Spatially Resolved Electronic Structure, Phys. Rev. Lett. **100**, 056807 (2008).
[13] B. Wang, M.-L. Bocquet, S. Marchini, S. Günther b, and J. Wintterlin, Chemical origin of a graphene moiré overlayer on Ru(0001), Phys. Chem. Chem. Phys. **10**, 3530 (2008).
[14] P. Sutter, M. S. Hybertsen, J. T. Sadowski, and E. A. Sutter, Electronic Structure of Few-Layer Epitaxial Graphene on Ru(0001), Nano Lett. **9**, 2654 (2009).
[15] I. Pletikosic, M. Kralj, P. Pervan, R. Brako, J. Coraux, A. T. NDiaye, C. Busse, and T. Michely, Dirac Cones and Minigaps for Graphene on Ir(111), Phys. Rev. Lett. **102**, 056808 (2009).
[16] A. Varykhalov, D. Marchenko, M. R. Scholz, E. D. L. Rienks, T. K. Kim, G. Bihlmayer, J. Sanchez-Barriga, and O. Rader, Ir (111) surface state with giant Rashba splitting persists under graphene in air, Phys. Rev. Lett. **108**, 066804 (2012).
[17] P. Sutter, J. T. Sadowski, and E. A. Sutter, Chemistry under Cover: Tuning Metal-Graphene Interaction by Reactive Intercalation, J. Am. Chem. Soc. **132**, 8175 (2010).

[18] C. Vo-Van, A. Kimouche, A. Reserbat-Plantey, O. Fruchart, P. Bayle-Guillemaud, N. Bendiab, and J. Coraux, Epitaxial graphene prepared by chemical vapor deposition on single crystal thin iridium films on sapphire, Appl. Phys. Lett. **98**, 181903 (2011).

[19] A. Kimouche, O. Renault, S. Samaddar, C. Winkelmann, H. Courtois, O. Fruchart, and J. Coraux Modulating charge density and inelastic optical response in graphene by atmospheric pressure localized intercalation through wrinkles, Carbon **68**, 73 (2014).

[20] A. Luican, G. Li, and E.Y. Andrei, Quantized Landau level spectrum and its density dependence in graphene, Phys. Rev. B **83**, 041405 (2011).

[21] S. Jung, G. M. Rutter, N. N. Klimov, D. B. Newell, I. Calizo, A. R. Hight-Walker, N. B. Zhitenev, and J. A. Stroscio, Evolution of microscopic localization in graphene in a magnetic field from scattering resonances to quantum dots Nature Phys. **7**, 245 (2011).

[22] Y. Zhang, V. W. Brar, F. Wang, C. Girit, Y. Yayon, M. Panlasigui, A. Zettl, and M. F. Crommie, Giant phonon-induced conductance in scanning tunnelling spectroscopy of gate-tunable graphene Nature Phys. **4**, 627 (2008).

[23] R. Larciprete, S. Ulstrup, P. Lacovig, M. Dalmiglio, M. Bianchi, F. Mazzola, L. Hornekaer, F. Orlando, A. Baraldi, P. Hofmann, and S. Lizzit Oxygen Switching of the Epitaxial Graphene Metal Interaction, ACS Nano **6**, 9551 (2012).

[24] Y.-W. Tan, Y. Zhang, K. Bolotin, Y. Zhao, S. Adam, E. H. Hwang, S. Das Sarma, H. L. Stormer, and P. Kim, Measurement of Scattering Rate and Minimum Conductivity in Graphene, Phys. Rev. Lett. **99**, 246803 (2007).

[25] A. Tomadin, M. Gibertini, F. Guinea, and M. Polini, *private communication.*

[26] G. Giovannetti, P. A. Khomyakov, G. Brocks, V. M. Karpan, J. van den Brink, and P. J. Kelly, Doping Graphene with Metal Contacts, Phys. Rev. Lett. **101**, 026803 (2008).

[27] G. M. Rutter, J. N. Crain, N. P. Guisinger, T. Li, P. N. First, and J. A. Stroscio, Scattering and interference in epitaxial graphene, Science **317**, 219 (2007).

[28] M. I. Katsnelson, K. S. Novoselov, and A. K. Geim, Chiral tunnelling and the Klein paradox in graphene, Nature Phys. **2**, 620 (2006).

[29] A. H. Castro-Neto, F. Guinea, N. M. R. Peres, K. S. Novoselov, and A. K. Geim, The electronic properties of graphene, Rev. Mod. Phys. **81**,109 (2009).

[30] C. Hwang, D. A. Siegel, S. Mo, W. Regan, A. Ismach, Y. Zhang, A. Zettl, and A. Lanzara, Fermi velocity engineering in graphene by substrate modification, Sci. Rep. **2**, 590 (2012).

[31] C. Faugeras *et al.,* Landau level spectroscopy of electron-electron interactions in graphene, arXiv:1412.0115v1 (2012).

[32] See Supplemental Material at ???